

## Chapter 5

### Measurements of $\beta$ and the Power Spectrum from the Las Campanas Redshift Survey

The Las Campanas Redshift Survey is one of the largest publicly available 3-dimensional galaxy catalogs. The selection criteria allowed the team to extract the largest number of galaxy redshifts given their telescope time. Unfortunately, this method of selecting targets makes the resulting survey more difficult to analyze. Although the catalog has been publicly available for nearly four years, there are no published real space power spectra. This is remarkable particularly since LCRS is still the publicly available catalog with the largest number of redshifts. By contrast, the IRAS PSCz catalog has been publicly available for less than a year and there are two available real-space power spectra (Tadros et al., 1999; Hamilton et al., 2000).

Matsubara et al. (2000) have made the most progress, by publishing an estimate for  $\beta$  (the amplitude of the redshift distortions),  $\sigma_8$  (the amplitude of the power spectrum) and  $\Gamma$  (a shape of the power spectrum). This parameterization allows for a partial characterization of the power spectrum. The parameterization does not reveal how well the data fit the simple model and may hide interesting features. As the measurements of cosmological parameters (from galaxy catalogs as well as other sources other sources) become more precise, these features become more interesting. Particularly interesting is the size scale ( $k$ ) at which the redshift distortions become nonlinear.

In chapter 4, I generalized the pair weight compression method to allow the analysis of redshift distortions and real space power spectra. The generalization calls for measuring (up to)

seven parameters at each separation

$$\xi^s(r) = \sum_{i=1}^7 \check{\xi}_i B_i(r_1, r_2, r_{12}) \quad (5.1)$$

where  $\xi^s(r)$  is the redshift space correlation function, each of the  $\check{\xi}_i$ 's is a measurable parameter and each of the  $B_i$ 's is function of the shape of the triangle formed by a galaxy pair and the observer. Each  $\check{\xi}_i$  can be transformed into a measure of  $P(k)$  and  $\beta$ . By properly combining the transformed  $\check{\xi}_i$ 's one is able to obtain measurements of, not only the galaxy-galaxy power spectrum ( $P(k)$ ), but also the galaxy-velocity ( $\beta P(k)$ ) and the velocity-velocity ( $\beta^2 P(k)$ ) power spectra. Unfortunately, chapter 4, also said that the measurements of  $\beta P(k)$  and  $\beta^2 P(k)$  are too imprecise to be measured without seriously reducing the number of independent estimates. Here I apply the pair weight method to the Las Campanas Redshift Survey to obtain a real space power spectrum. Then using this power spectrum as the shape of the true power spectrum, I perform a least-squares fit to the amplitude of the power spectrum and  $\beta$ .

## 5.1 Real Space Power Spectrum

Figure 5.1 shows the correlated real space power spectrum as derived by the pair weight method. The error bars on the real space power spectrum are larger than those for the redshift space power spectrum. This is to be expected since there are now more parameters to fit with the same information. The real space power spectrum appears to be similar to the redshift space counterpart. Due to aliasing at the large  $k$  end (see Figure 3.2), and inaccuracy at the low  $k$  end, the inner half of the points (from  $k = .1 - .3$ ) of both curves should be considered to be the most reliable. The similarity in amplitude of the real space power spectrum and the redshift space power spectrum would imply a low value of  $\beta$ .

The calculation of this estimate only uses shape functions 0, 2 and 4 as defined in Appendix A. The inclusion of additional shape functions reduced the quality of the estimate. That is to say that, not only was the estimate less believable, but the error bars were enlarged. When calculating the Fisher matrix with Monte Carlo techniques, there are inevitably errors in some

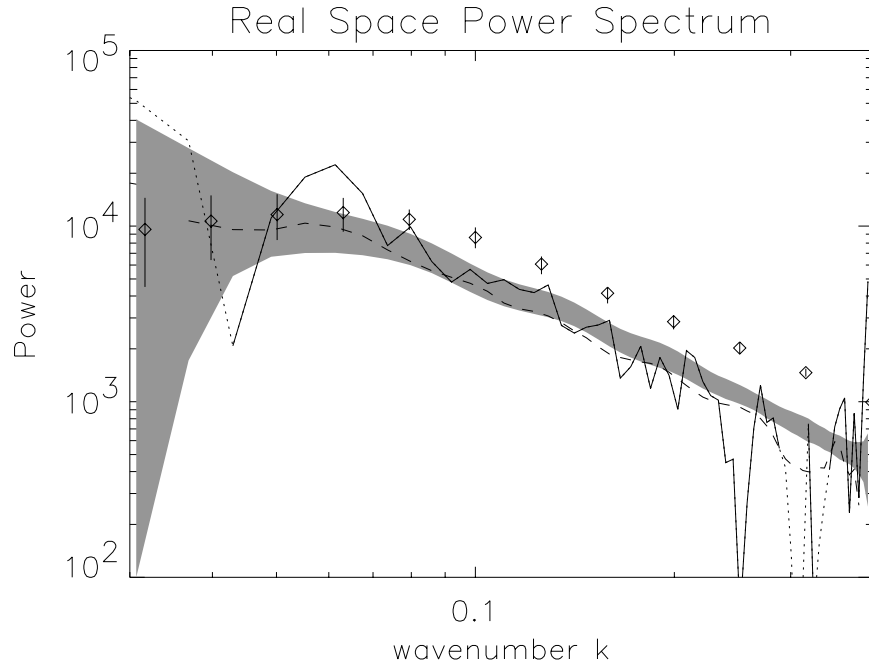


Figure 5.1: Power spectrum of the cut catalog’s 21996 LCRS galaxies. The solid line shows where the measured real space power spectrum is positive. The line is dotted where either end of the segment is negative. The shaded region is the expected error about the prior power spectrum. The dashed line is the redshift space power spectrum. The diamonds with error bars is the redshift space power spectrum measured by Lin et al. (1996b).

of the matrix elements. Unfortunately, when the matrices are inverted these errors can dominate the calculation. In particular, errors in the off diagonal terms involving  $\Xi_{0, 2 \text{ or } 4}$  and  $\Xi_{1, 3, 5 \text{ or } 6}$  can contaminate the calculation of the estimates of  $\Xi_{0, 2 \text{ or } 4}$ . It is also true that the scatter in the measurement using only shape function 0, 2, and 4 is larger than the calculated error. This can be seen in Figure 5.1. The fluctuations in the correlated power spectrum are larger than the predicted errors (shaded region) especially at the large  $k$  end. This is addressed in the following section.

## 5.2 Calculated Errors

The fluctuations in the measurements of neighboring points is empirically larger than the error bars calculated from the Fisher matrix. It is clear that part of the problem is that high

covariances between the measurements of two parameters gives a lower measurement of the error than is reasonable. In addition to this, miscalculation of Fisher matrix elements increases the problem. We have not yet been able to correct the error bars to reflect the true level of the errors. In the remainder of this Chapter, we use an empirically calculated, multiplicative factor to increase the level of the errors. That is to say, we use the relative scatter in the nominal “unit variance” calculation as the correction factor.

### 5.3 Measurement of $\beta$

Figure 4.4 shows that the amount of information in any one estimate of  $\beta P(k)$  or  $\beta^2 P(k)$  is very low. For this reason, to find the best estimate for  $\beta$  it is important to use all the available information. On the smallest scales, however, nonlinearities may become important. The most likely result of nonlinear contamination is that the estimate of  $\beta$  would be reduced. This is because the linear model for redshift distortions squashes structures along the line of sight. However, on the smallest scales the “fingers of God” clearly stretch structures along the line of sight. At the same time, however, these bins at large  $k$  will also be contaminated by aliasing. For these reasons, the calculation for the most likely value of  $\beta$  is performed at each wavenumber by including information cumulatively up to that wavenumber. If nonlinearities become important then  $\beta$  should drop perceptibly at large wavenumbers.

Figure 5.2 shows the best fit value of  $\beta$  for each wavenumber. In each case, the power spectrum is assumed to have the shape of the measured correlated power spectrum. The first six bins of the power spectrum have (unphysical) negative values. The power spectrum in these bins is not accurately measured. For this reasons, these bins have been ignored for all of the calculations. In each calculation, the only measured parameters are the amplitude of the power spectrum and  $\beta$ . As expected, as more data is added to the calculation the variation in the best measurement is reduced. Figure 5.2 shows no conclusive evidence for entering the nonlinear regime. This is only slightly surprising since the smallest length scale probed is  $8h^{-1}\text{Mpc}$  and the location where one would expect to see nonlinearities is also affected by aliasing.

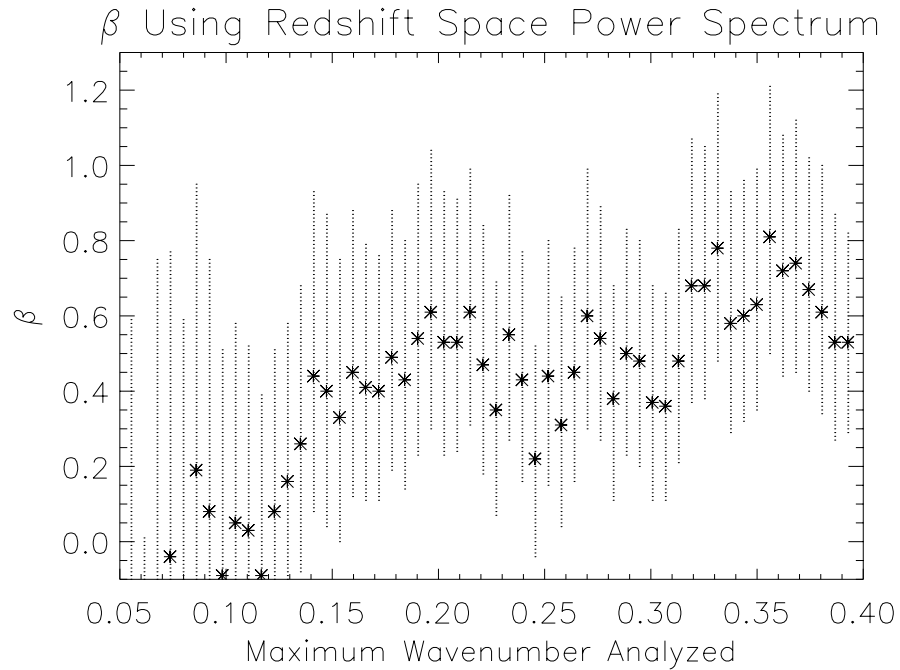


Figure 5.2: This Figure shows the  $1 - \sigma$  errors and best fit for  $\beta$  using the amplitude of the correlated power spectrum as the only other free parameter. At each plotted wavenumber, the fit uses information at smaller wavenumbers only. The stars show the best fit value for  $\beta$  at each wavenumber.

Figure 5.3 shows the best fit value for the measurement of the amplitude of the correlated power spectrum. As expected, as more information is added to the calculation the amplitude of the power spectrum becomes less uncertain and the value tends toward unity. This means that the best measured amplitude for the decorrelated power spectrum is the same as for the correlated power spectrum.

At each wavenumber the amplitude and the value of  $\beta$  are highly anti-correlated. Figure 5.4 shows the typical error region in the amplitude- $\beta$  plane. The marginalized  $1 - \sigma$  error in each parameter is the most extreme value along the  $1 - \sigma$  contour. This marginalized error is the error bar plotted in Figures 5.2 and 5.3.

The final result is that the amplitude of the correlated, real space power spectrum should be  $1. \pm .25$  times the curve shown in Figure 5.1 and  $\beta \approx 0.55^{+.35}_{-.30}$ . This value is obtained from

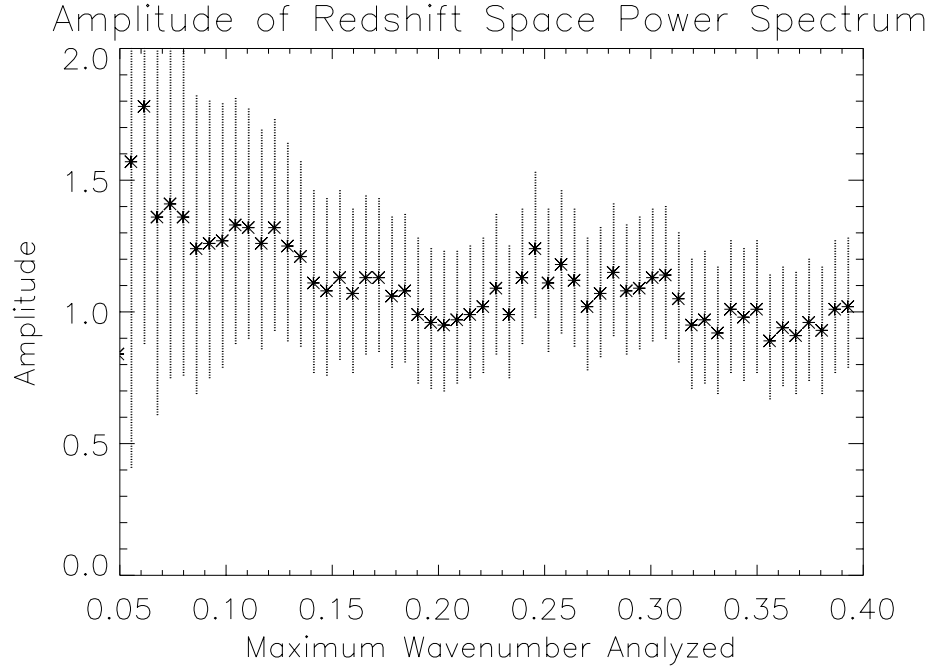


Figure 5.3: This figure shows the best fit amplitude and the  $1 - \sigma$  error for the amplitude of the correlated power spectrum. At each wavenumber, the fit uses only information from smaller wavenumbers. The only other free parameter is  $\beta$ .

the best overall fit at  $k = .209h\text{Mpc}^{-1}$ . This is a good choice because it uses as much of the linear information as possible while not being contaminated by aliasing.

#### 5.4 Discussion and Conclusions

The pair weight compression method is able to extract a real space power spectrum and an estimate of  $\beta$  from LCRS. Unfortunately, only three of the seven shape functions yielded useful results. In fact, including the additional shape functions provided an estimate that was clearly incorrect. In order to include information from all seven shape functions it is necessary to calculate all of the matrix elements in the Fisher matrix to adequate precision. For this calculation, the monopole-monopole elements were calculated to expected errors of 2.5 percent. The off-diagonal elements typically had errors of a few percent but routinely there were elements with errors of tens of percent. Reducing the calculation to only those shape functions which

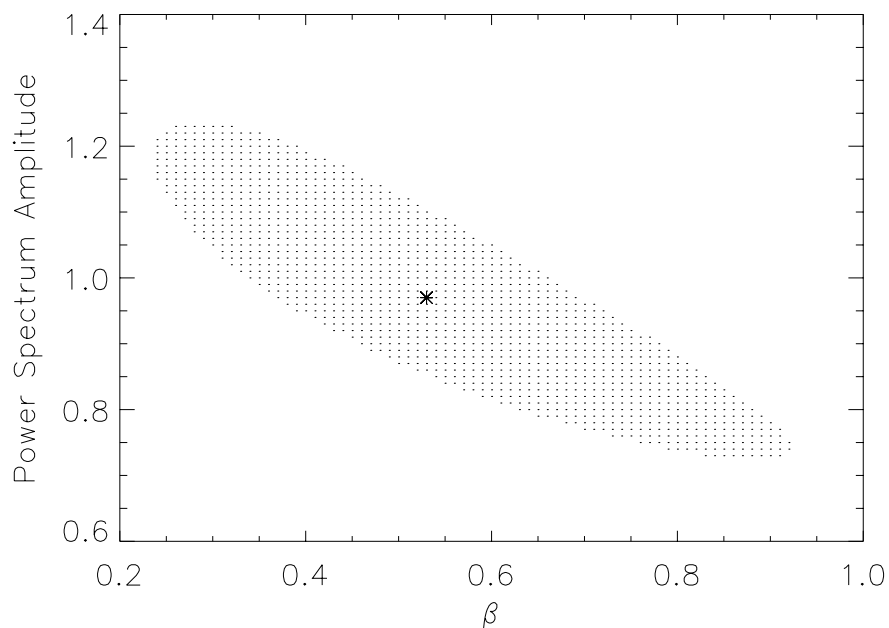


Figure 5.4: The  $1-\sigma$  error region for the calculation including all wavenumbers up to  $k = 0.209 \text{ h Mpc}^{-1}$ . The star is the best fit value.

are non-zero at small separations, reduced the errors caused by the off-diagonal terms. However, the scatter in the calculated estimates were still larger than the calculated error bars. As a result, the real space power spectrum is noisier than the redshift space power spectrum. This would be true even if the Fisher matrix were calculated exactly because the same information is now being shared amongst three estimates. The resulting real space power spectrum has similar shape to the redshift space power spectrum. This is not at all surprising since a majority of the analysis is on wavenumbers which should not be greatly affected by nonlinearities.

The estimate of  $\beta \approx .55_{-.30}^{+.35}$  is consistent with a flat low matter density universe. In particular, it is consistent with the estimates from rich clusters (Carlberg et al., 1998) and cosmic microwave background measurements (de Bernardis et al., 2000). A flat matter dominated universe is once again ruled out unless the bias factor is rather large. Although the estimate of  $\beta$  is larger than that of Matsubara et al. (2000) ( $\beta = .30 \pm .39$ ) the estimates are consistent within

the errors.